

# Anisotropic van der Waals Dispersion Forces in Polymers: Structural Symmetry Breaking Leads to Enhanced Conformational Search

Mario Galante and Alexandre Tkatchenko

*Department of Physics and Materials Science, University of Luxembourg, L-1511 Luxembourg City, Luxembourg*

(Dated: October 14, 2021)

The modeling of conformations and dynamics of (bio)polymers is of primary importance for understanding physicochemical properties of soft matter. Although short-range interactions such as covalent and hydrogen bonding control the local arrangement of polymers, non-covalent interactions play a dominant role in determining the global conformations. Here we focus on how the inclusion of many-body effects in van der Waals dispersion affects the outcome of geometry optimizations and molecular dynamics simulations of model polymers. We find that delocalized force contributions are key to explore the conformational landscape, as they induce an anisotropic polarization response which efficiently guides the conformation towards globally optimized structures. This is in contrast with the commonly used pair-wise approach, where the atomic polarizabilities lack information on the global geometry. We show that such local approximation causes the conformational search to be obstructed by conformations with unphysically limited spatial symmetry, while the many-body formalism strongly reduces the roughness of the potential energy landscape.

The prediction of structure formation in polymers under realistic thermodynamical conditions is a challenging problem that is relevant for fields ranging from medicine and biology to physics and engineering. For example, the folding of proteins into their secondary structure underpins the regulation of many functions of cellular activity [1]. In addition, the ubiquitous presence of polymeric materials in countless modern applications is due to their variety of physical macroscopic properties which are in turn dictated by polymer morphology and its time evolution [2–4]. However, conformational stabilities are easily undermined by thermal fluctuations and the solvent environment, therefore non-equilibrium effects are drastically relevant in determining the typical configurations as well as the dynamical time scales [5–7]. In principle, all relevant information on dynamical transitions between conformations can be evinced by the free energy landscape [8]. Nevertheless, the exhaustive sampling of such a high-dimensional surface becomes prohibitively expensive for realistic systems, where several thousands of degrees of freedom have to be included. Consequently, many investigations of polymeric conformations rely on simplified mathematical models to represent a given polymeric arrangement and probe the conformational space by means of statistical mechanics tools [9].

An appropriate estimation of the physical interactions is however essential in order to perform conformational searches with feasible computational costs [10–12]. Many methods were proposed [13, 14], where the general physical model includes short range specific forces to represent covalent bonding together with additional longer ranged potentials to account for unspecific forces such as van der Waals (vdW) interactions. The latter play a dominant role in determining the global arrangement because of their strikingly slower spatial decay. They are normally included by means of the pair-wise (PW) approximation, where the energy decays strictly with the 6th power of

the interatomic distance and its strength is dictated by the local chemical environments [15–17]. However, recent investigations [18–21] have shown that the fixed (and relatively short) interaction range together with the lack of non-locality and many-body effects makes the PW approximation not suitable to adequately capture the complexity of dispersion interactions in a variety of systems.

In this Letter we present numerical evidence that the inclusion of many-body dispersion interactions is essential to explore polymer conformations. In fact, we show that the independence of the PW polarizability on the global structure yields forces that are not capable of breaking the spatial symmetry of particular polymer arrangements, thus wrongly overestimating their stability. On the contrary, a formulation of van der Waals interactions that includes many-body effects naturally includes anisotropic delocalized polarization response that drives conformations towards globally optimized geometries. We show that this is intimately related to the significantly longer range and the entropic nature of the forces, and that these aspects are a direct consequence of the non-locality of polarization response. In addition, we find that PW forces artificially enhance the roughness of the potential energy landscape, and therefore imply a reduced efficiency of the conformational search. We note that the smoothening of the landscape with the increasing of the interaction range has already been shown in the context of PW potentials [22–26].

Our system of choice is a carbon-based polymer represented by the model Hamiltonian

$$\mathcal{H} = \sum_{i=1}^{N-1} k \left( \left| \mathbf{R}_i - \mathbf{R}_{i+1} \right| - R_0 \right)^2 + \sum_{i=1}^N \sum_{j \neq i, i \pm 1} a \exp \left\{ -b \left| \mathbf{R}_i - \mathbf{R}_j \right| \right\} + E_{\text{vdW}}, \quad (1)$$

with  $\mathbf{R}_i$  representing the position of the  $i$ th carbon atom,

$k = 39.57$  a.u. ,  $a = 1878.38$  a.u. and  $b = 5.49$  a.u. . The first term represents an harmonic covalent bond between the nearest-neighbours, while the second summation introduces a Born-Mayer repulsive potential between non-nearest-neighbours that prevents artificial agglomeration of the polymer. We remark that the harmonic potential only bounds the atoms to oscillate around the equilibrium inter-atomic distance,  $R_0 = 1.52$  Å, therefore the only factor that introduces an angular dependence of the atomic bonds is the vdW energy,  $E_{\text{vdW}}$ . The latter can be generally expressed by means of the adiabatic connection fluctuation-dissipation (ACFD) formula [27, 28],

$$E_{\text{vdW}}^{\text{MBD}} = \frac{\hbar}{2\pi} \int_0^\infty du \int_0^1 d\lambda \int \int d\mathbf{r} d\mathbf{r}' \quad (2)$$

$$\times \text{tr} \left[ (\boldsymbol{\alpha}_\lambda(\mathbf{r}, \mathbf{r}', iu) - \boldsymbol{\alpha}_0(\mathbf{r}, \mathbf{r}', iu)) \mathbf{T}(\mathbf{r}, \mathbf{r}') \right],$$

where  $\mathbf{r}$ ,  $\mathbf{r}'$  are spatial variables,  $u$  is the frequency of the electric field,  $\text{tr}$  denotes the trace of the polarizability tensors,  $\boldsymbol{\alpha}$ , and the integral over the coupling strength,  $\lambda$ , expresses the adiabatic switching-on of the electron-electron interaction. Here we approximate the ACFD equation within the many-body dispersion (MBD) approach [28, 29] and we define the coupling tensor,  $\mathbf{T}$ , as the dipole-dipole potential corresponding to two Gaussian charge distributions. The polarizability tensor of the system corresponding to uncorrelated atoms,  $\boldsymbol{\alpha}_0$ , can be written as the sum of the polarizabilities localized at each atomic site,

$$\boldsymbol{\alpha}_0(\mathbf{r}, \mathbf{r}') \approx \sum_i \delta^3(\mathbf{r} - \mathbf{R}_i) \delta^3(\mathbf{r}' - \mathbf{r}') \mathbb{1}_3 \alpha_i^{\text{TS}}, \quad (3)$$

where  $\alpha_i^{\text{TS}}$  accounts for all short range correlations and is here taken as the isotropic atomic polarizability for a generic carbon calculated within the Tkatchenko-Scheffler (TS) scheme [15],  $\alpha_C^{\text{TS}} = 10.44$  a.u. The polarizability of the interacting system,  $\boldsymbol{\alpha}_\lambda$ , can then be calculated through the Dyson-like screening equation,

$$\boldsymbol{\alpha}_\lambda = \sum_{n=0}^{\infty} \langle \boldsymbol{\alpha}_0 (-\lambda \mathbf{T} \boldsymbol{\alpha}_0)^n \rangle, \quad (4)$$

which allows to construct a non-local tensor starting from the local atomic polarizabilities. We remark that the solution of Eqs. (2) and (4) within these approximations correspond to solving the Schrödinger equation for a system of quantum harmonic oscillators centered at the atomic sites and coupled via the dipole-dipole potential [27]. As a consequence, the MBD formalism accounts for the energy of global charge oscillations expressed through linear combinations of the atomic dipolar displacement vectors. In other terms, the MBD energy is the sum of the interaction energies of the  $3N$  normal modes, with  $N$  being the total number of oscillators. In contrast, the PW approximation corresponds to truncating the series of Eq. (4) to

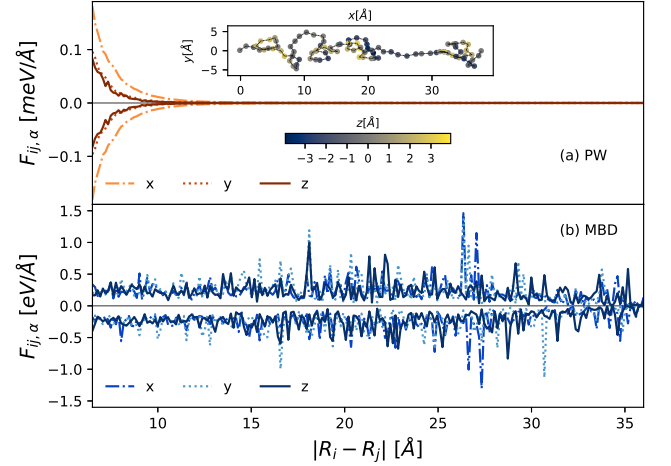


FIG. 1. (Color Online) Dependence of the averaged pair-wise (a) and many-body (b) force components for the interatomic distance for a conformation obtained through molecular dynamics for a 100 atoms chain (shown in the inset).

the second order and considers only unscreened dipole-dipole interactions,

$$E_{\text{vdW}}^{\text{PW}} = -\frac{1}{2} \sum_{i \neq j} f_{\text{damp}}(R_{ij}) \frac{C_{6,ij}}{R_{ij}^6}, \quad (5)$$

where  $f_{\text{damp}}$  is a Fermi-type damping function that eliminates short range contributions and  $C_{6,ij} = \frac{3}{\pi} \hbar \int du \alpha_i^{\text{TS}}(iu) \alpha_j^{\text{TS}}(iu)$ .

We begin by analyzing the differences between the long range behavior of the components of the PW and MBD forces for a representative conformation of a 100 atoms chain extracted from a molecular dynamics (MD) trajectory [Fig. 1]. The PW force between a given pair of atoms can be calculated analytically from Eq. 5 and therefore follows by construction the  $R^{-7}$  power law, becoming negligible within 20 Å. On the contrary, the MBD force is the result of the competition between all global oscillation modes of the coupled dipoles. Here we numerically calculate the contribution acting on the  $i$ -th site coming from the  $j$ -th atom by using the formula,

$$F_{ij,\alpha}^{\text{MBD}} = -\frac{\partial}{\partial R_i^\alpha} \sum_{m=1}^{3N} [\varepsilon_m \chi_j^m], \quad \chi_j^m = \sqrt{\sum_{\alpha=x,y,z} (\chi_{j,\alpha}^m)^2} \quad (6)$$

where  $\varepsilon_m$  is the eigenvalue of the  $m$ -th MBD mode, and  $\chi_{j,\alpha}^m$  is the  $\alpha = x, y, z$  component of the displacement vector of the  $j$ -th dipole within the same mode. From panel (b) it is evident that the average contribution to MBD forces is entropically scattered throughout the whole distance range and no clear decay rate can be singled out. This can be attributed to the elevated degree of delocalization of the MBD eigenmodes, as shown in Ref. [19]. Moreover, the persistence of MBD interactions for long

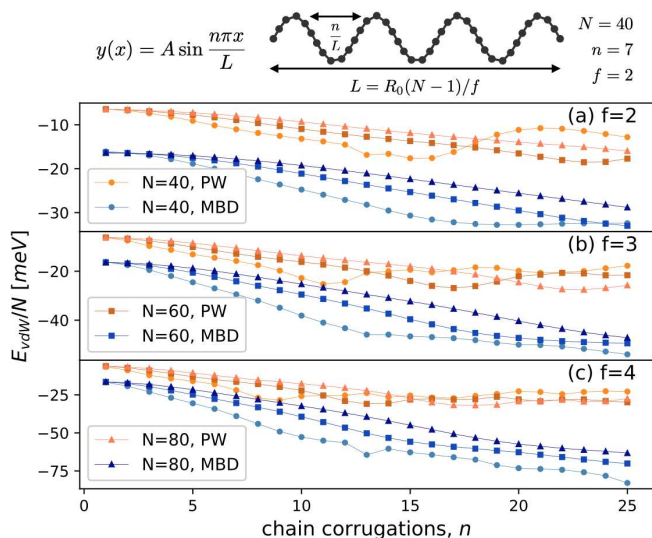


FIG. 2. (Color Online) Top: schematics for initialization of 2D chain conformation. Panels (a)-(c): vdW energy per atom against the number of chain corrugations,  $n$ , for 40, 60 and 80 atoms and for compression factors  $f = 2, 3, 4$ .

distances has already been reported in model and realistic systems [20, 30], and their structure dependence will be analyzed in future publications. Furthermore, there is no evident relation between the MBD force components and the (cylindrical-like) spatial geometry of the conformation. This is in contrast with the PW case, where the longitudinal ( $x$ ) component is more pronounced than the others. We also remark that the typical contribution at a given distance is three orders of magnitude higher for MBD than for PW forces, although in both cases contributions of opposite sign balance to yield an average atomic force of  $\approx 0.01$  eV/Å. This can be associated to the interplay between the contributions due to the  $3N$  normal modes, in consistency with the analysis of the atomic force response presented in Ref. [30].

We now focus on how each approximation explores the configurational space starting from the same two-dimensional conformations. We define our structures by distributing  $N$  atoms along the curve  $y(x) = A \sin(n\pi x/L)$ , where the spatial frequency,  $n$ , and the end-to-end distance,  $L$ , are input parameters. For convenience, we quantify  $L$  in terms of fractions of the length of a one-dimensional chain of equispaced atoms, namely  $L = R_0(N-1)/f$ , with  $f > 1$ . The amplitude,  $A$ , is then calculated numerically so that the average of the inter-atomic distances along the function  $y(x)$  is equal the equilibrium spacing,  $R_0$ . This choice allows us to consider a regular and systematically reproducible input structure, which is however not exactly symmetric. Figure 2 displays how  $n$  influences the vdW energy per atom for a series of chains with different number of atoms and compression factors,  $f$ . Here orange (blue) data points

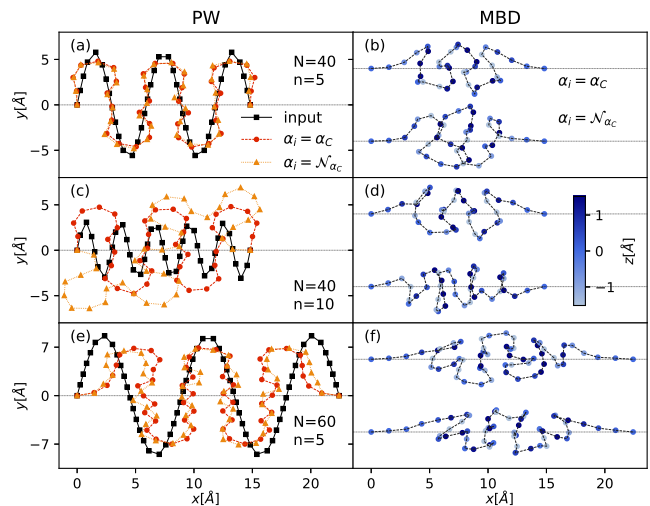


FIG. 3. (Color Online) Left panels: comparison between a 40 atoms sinusoidal conformation (black triangles) and the results of geometry optimizations performed within the PW approximation the vdW energy for  $f = 4$  and  $(N, n) = (40, 5)$ ,  $(40, 10)$  and  $(60, 5)$ , respectively. Red circles represent atoms in a chain with atomic polarizabilities set to  $\alpha_C^{\text{TS}} = 10.44$ , while orange squares refer to atoms with polarizabilities that were generated according to a normal distribution,  $\mathcal{N}_{\alpha_C}$ , centered at  $\alpha_C^{\text{TS}}$  with a 30% variance. Right panels: the results of MBD energy optimization for the same input structures shown in the corresponding left panels. The color coding here represents the magnitude of the  $z$  coordinates. In each panel the top (bottom) structure displays a chain with constant (irregular) atomic polarizability.

refer to the PW (MBD) approach, convention that is maintained throughout the paper. It is clear that the trends of the PW energy generally present local minima and saturate for the most corrugated (higher  $n$ ) structures. In contrast, MBD energies monotonically decrease in all cases, exception made for  $N = 40$  chains, where the irregularity is due to the low number of atoms and their irregular distribution across the sinusoidal function. This difference is particularly pronounced for the more compressed conformations [panels (b) and (c)], meaning that MBD generally favours arbitrarily high corrugation rather than admitting specific preferred values for the spatial frequency. Therefore, this result is a first indication that the potential energy surface associated with the PW energy is characterized by a higher number of local minima with respect to MBD.

We continue by presenting the outcome of geometry optimizations of some representative two-dimensional chain conformations, represented by the black curves in the left panels of Fig. 3. For simplicity, we constrain the position of the two edge atoms at the fixed (input) distance. We find that all PW optimized structures (orange curves, left panels) consistently yield conformations that remain within the input plane,  $z = 0$ , while MBD consistently produces three-dimensional helical-like structures

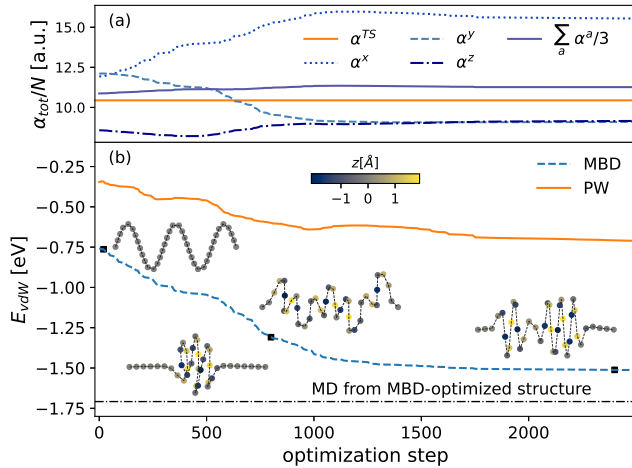


FIG. 4. (Color Online) Evolution of the vdW energy (top) and of the average atomic polarizability,  $\alpha$ , along an MBD optimization path. Panel (a): the dashed blue (solid orange) curve represents the trend of the MBD (PW) energy with the progression of the optimization. The dot-dashed line indicates the energy of the conformation (displayed on the bottom left) obtained through a MD simulation starting from the MBD optimized structure. The black squares denote the vdW energy and optimization step of the remaining three conformations displayed. Panel (b): the orange solid line represents the input atomic polarizability,  $\alpha_C^{\text{TS}}$ , while the dotted, dashed and dot-dashed lines correspond to the  $x$ ,  $y$  and  $z$  components of the average atomic polarizability, respectively.

(right panels). We also display the analogous results for chains with atomic polarizabilities irregularly distributed according to a Gaussian,  $\mathcal{N}_{\alpha_C}$ , with mean  $\alpha_C^{\text{TS}}$  and a variance of 30%, which display the same qualitative (and often quantitative) outcome. The discrepancy between the two models is a direct consequence of the higher versatility of the MBD polarizability tensor with respect to the PW polarizability, as it accounts for anisotropic polarization response. In fact, the interaction between isotropic dipolar fluctuations, as considered within the PW approach (Eq. (3)), is purely of radial character by construction. Nevertheless, this is no longer true when one considers a screened polarization response, which effectively introduces an anisotropy in the atomic polarization tensors. We further analyze this by evaluating the polarizability tensor by means of the Dyson-like equation of Eq. (4) for  $\lambda = 1$  (its trace corresponding to experimentally measured polarizability). In Fig. 4 (a) we display the average atomic polarizability along the Cartesian directions,

$$\alpha_{\text{tot}}^a = N^{-1} \sum_{ij} \sum_b \alpha_{\lambda=1}^{ab}(\mathbf{R}_i, \mathbf{R}_j), \quad (7)$$

calculated for the conformations along the MBD optimization path of a representative structure. It is clear that the screened atomic total polarizability remains

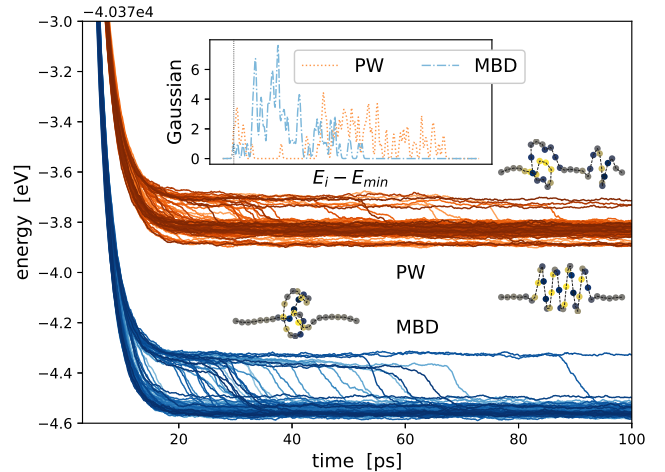


FIG. 5. (Color Online) Results of MD simulations (100 per vdW model) at 5 K for a 40 atoms chain starting from the 2D conformation defined by  $n = 5$  and  $f = 2$ . Orange (blue) lines represent the evolution of the total energy with time for the PW (MBD) approximation of the vdW energy. The structures on the right represent the steady-state PW conformations with the highest (top) and the lowest (bottom) energy, while the structure on the left is a typical MBD steady-state structure. The inset shows the Gaussian distributions centered steady-state energies for a each vdW model, rescaled by  $E_{\min} = \min\{E_i\}$  and normalized so that they peak at 1.

mostly constant throughout the optimization, while the PW atomic polarizability is fixed to  $\alpha_C^{\text{TS}}$ . However, the components of the total screened polarizability gradually change to reproduce the cylindrical-like symmetry imposed by the constrain on the position of the edge atoms, with the longitudinal ( $x$ ) component growing dominant with respect to the others. We remark that this is analogous to the asymmetry of the force components observed in Fig. 1, and it is evident that the anisotropic character of MBD atomic polarizabilities is responsible for driving the structure towards a three-dimensional conformation. In fact, the change in the symmetry of the total polarizability goes on equal footing with the lowering of the MBD energy, as shown in Fig. 4 (b). For comparison, we display the PW energy calculated for the structures encountered on the MBD optimization path. We find that the trend of the latter presents two local minima, the first of which corresponding to the point where the conformation starts to deviate from the input plane. This indicates that a transition to a three-dimensional conformation can be obtained only if external interactions are considered together with the PW forces. Namely, this result suggests that the assumption of isotropic atomic polarizabilities leads to additional energy barriers that may obstacolate the conformational search.

We expand our exploration of the conformational space of the polymer by considering 100 MD trajectories for each vdW model, all run at 5 K and starting from the

2D conformation of a 40 atoms chain defined by  $n = 5$  and  $f = 2$ . Despite the very low temperature, we argue that these results should be considered valid for a realistic polymer at much higher temperatures. In fact, the average vdW energy per atom in realistic supramolecular systems is normally much higher than the one of the present models, as here we consider a much more limited number of degrees of freedom. For example, the PW energy per atom of helical poly-alanines calculated in Ref. [31] is roughly 35 times larger than the one of the typical model chain here considered. Therefore, assuming that the height of the energy barriers between minima undergoes the same scaling of the total energy, the thermal fluctuations introduced in a 5 K dynamics in our model systems correspond to exploring the PES at 175 K for a realistic polymer. In addition, the conformational stability of realistic systems is given by the cooperation between vdW interactions and a number of other factors, which are here neglected. Therefore, we argue that such interplay may further enhance the influence of vdW forces and consequently make our considerations applicable to realistic systems at substantially higher temperatures.

In Fig. 5 we display the time evolution up to 100 ps of the total energy for all MD trajectories. While the vast majority of the simulations produced steady-state structures with total energies of similar magnitude, a small portion converges to irregular structures corresponding to local minima at higher energies. Given the scarcity of such events, we choose to exclude from the analysis the trajectories with the 5 highest steady-state energies as we consider them not representative. The inset display the Gaussian-broadened distribution of the local minima that the remaining 95 trajectories (per model) converge to. It is clear that PW trajectories yield a large variety of steady-state energies, with the lowest energies distinctly separated from the others, while MBD energies are more condensed towards the absolute minimum,  $E_{\min}$ . To quantify this difference we calculated the roughness of the free energy landscape, defined as the root-mean-squared energy distance from  $E_{\min}$ ,  $\langle (E - \min\{E\})^2 \rangle^{1/2}$  [32], which gives  $\sim 137 k_B T$  and  $\sim 63 k_B T$ . This result shows that the PW energy landscape has more than twice the roughness of the MBD one, meaning that assuming a local polarizability tensor increases the probability of obtaining steady-state conformations that are far from the absolute minimum. Moreover, 19 of the MBD trajectories undergo a transition after the initial transient ( $t \gtrsim 20$  ps), while this occurs only in 10 cases for PW. Although the height of the energy barriers is roughly similar ( $\approx 10$  meV), MBD transitions have average longer duration ( $\approx 34$  ps against 23 ps) and result in a larger energy decrease ( $\approx 0.21$  eV against 0.15 eV). Therefore, we can conclude that the non-locality of the polarizability tensor significantly improves the conformational search efficiency. We remark that this is consistent with other

investigations on conformational searches lead by global non-specific interactions [33–36].

Finally, we compare the PW structure with the lowest steady-state energy (bottom right of Fig. 5) with a typical MBD steady-state conformation (left). The helical-like PW conformation is asymmetric in all three Cartesian direction, in contrast with the knot-like MBD structure which sacrifices the local regularity in favor of a cylindrical-like symmetry. This is an additional evidence that the inclusion of many-body effects guides the structure formation towards global geometries that reflect the spatial symmetry dictated by the environment. Furthermore, we have shown that MBD improves the efficiency of the conformational search as the roughness of the potential energy landscape is decreased, while the higher stability of MBD-optimized structures was already demonstrated in the context of molecular crystal [37]. Therefore, we can conclude that many-body dispersion interactions are key to stabilize polymer conformations that are consistent with the geometrical symmetry imposed by the environment, and they should be considered in generic conformational searches.

The authors acknowledge support from the ERC Consolidator Grant “BeStMo”. MG is grateful to Marco Pezzutto and Matteo Gori for many fruitful discussions.

- 
- [1] Z. Bu and D. J. Callaway, in *Protein Structure and Diseases*, Advances in Protein Chemistry and Structural Biology, Vol. 83, edited by R. Donev (Academic Press, 2011) pp. 163–221.
  - [2] B. Adhikari and S. Majumdar, *Prog. Polym. Sci.* **29**, 699 (2004).
  - [3] R. Dersch, M. Steinhart, U. Boudriot, A. Greiner, and J. Wendorff, *Polym. Adv. Technol.* **6**, 276 (2005).
  - [4] B. Ulery, L. Nair, and C. Laurencin, *Polym. Adv. Technol.* **49**, 832 (2011).
  - [5] S. Napolitano, *Non-Equilibrium Phenomena in Confined Soft Matter* (Springer, 2015).
  - [6] J. S. Fraser, M. W. Clarkson, S. C. Degnan, R. Erion, D. Kern, and T. Alber, *Nature* **462**, 669 (2009).
  - [7] V. N. Uversky, in *Protein Folding and Misfolding: Neurodegenerative Diseases*, edited by J. Ovádi and F. Orosz (Springer, 2009) pp. 21–75.
  - [8] D. J. Wales, *Energy Landscapes: Applications to Clusters, Biomolecules and Glasses* (Cambridge University Press, 2003).
  - [9] Z. G. Wang, *Macromolecules* **50**, 9073 (2017).
  - [10] C. Levinthal, in *Mossbauer Spectroscopy in Biological Systems, Proceedings of a Meeting held at Allerton House, Monticello, Illinois* (University of Illinois Press, 1969) p. 22.
  - [11] R. Zwanzig, A. Szabo, and B. Bagchi, *PNAS* **89**, 20 (1992).
  - [12] M. Karplus, *Fold. Des.* **2**, S69 (1997).
  - [13] H. D. Tran and R. Ramprasad, *J. Phys. Chem. Lett.* **11**, 5823 (2020).
  - [14] S. Abeln, K. A. Feenstra, and J. Heringa, in *Encyclope-*

- dia of Bioinformatics and Computational Biology*, Vol. 2, edited by S. Ranganathan (Elsevier, 2019) p. 497.
- [15] A. Tkatchenko and M. Scheffler, *Phys. Rev. Lett.* **102**, 73005 (2009).
- [16] T. Sato and H. Nakai, *J. Chem. Phys.* **131**, 224104 (2009).
- [17] S. Grimme, J. Antony, S. Ehrlich, and H. Krieg, *J. Chem. Phys.* **138**, 154104 (2010).
- [18] J. F. Dobson, *Int. J. Quantum Chem.* **114**, 1157 (2014).
- [19] A. Ambrosetti, N. Ferri, R. A. DiStasio Jr., and A. Tkatchenko, *Science* **351**, 1171 (2016).
- [20] M. Stöhr and A. Tkatchenko, *Sci. Adv.* **5**, eaax0024 (2019).
- [21] P. Hauseux, T. Nguyen, A. Ambrosetti, K. S. Ruiz, S. P. A. Bordas, and A. Tkatchenko, *Nat. Commun.* **11**, 1651 (2020).
- [22] M. R. Hoare and J. McInnes, *J. Chem. Soc.* **61**, 12 (1976).
- [23] M. R. Hoare and J. McInnes, *Adv. Phys.* **32**, 791 (1983).
- [24] J. P. K. Doye and D. J. Wales, *J. Chem. Phys.* **105**, 84228 (1996).
- [25] M. C. Rechtsman, F. H. Stillinger, and S. Torquato, *Phys. Rev. Lett.* **95**, 228301 (2005).
- [26] M. C. Rechtsman, F. H. Stillinger, and S. Torquato, *Phys. Rev. E* **73**, 011406 (2006).
- [27] J. Hermann, R. A. DiStasio Jr., and A. Tkatchenko, *Chem. Rev.* **117**, 4714 (2017).
- [28] A. Tkatchenko, A. Ambrosetti, and R. A. DiStasio Jr., *J. Chem. Phys.* **138**, 074106 (2013).
- [29] A. Tkatchenko, R. A. DiStasio Jr., R. Car, and M. Scheffler, *Phys. Rev. Lett.* **108**, 236402 (2012).
- [30] P. Hauseux, A. Ambrosetti, S. P. A. Bordas, and A. Tkatchenko, (2021), preprint at <https://arxiv.org/abs/2106.08113>.
- [31] A. Tkatchenko, M. Rossi, V. Blum, J. Ireta, and M. Scheffler, *Phys. Rev. Lett.* **106**, 118102 (2011).
- [32] L. Milanese, J. P. Waltho, C. A. Hunter, D. J. Shaw, G. S. Beddard, G. D. Reid, S. Dev, and M. Volk, *PNAS* **109**, 19563 (2012).
- [33] D. Osmanovic and Y. Rabin, *J. Chem. Phys.* **144**, 205104 (2016).
- [34] A. Chakrabartty and R. L. Baldwin, *Adv. Prot. Chem.* **46**, 141 (1995).
- [35] B. M. P. Huyghues-Despointes, T. M. Klinger, and R. L. Baldwin, *Biochemistry* **34**, 13267 (1995).
- [36] S.-S. Sung, *Prot. Sci.* **26**, 2003 (2017).
- [37] A. M. Reilly and A. Tkatchenko, *Phys. Rev. Lett.* **113**, 0655701 (2014).